



Deep Throttle of a Nitrous Oxide and Hydroxyl-Terminated Polybutadiene Hybrid Rocket Motor

Stephen A. Whitmore,* Zachary W. Peterson,† and Shannon D. Eilers†

Utah State University, Logan, Utah 84322

DOI: 10.2514/1.B34967

Deep-throttle static test results from an N₂O and hydroxyl-terminated polybutadiene hybrid rocket motor are presented. The nominal 800 N thrust level was turned down to less than 12 N while still maintaining stable and controlled combustion. This 67:1 turndown was accomplished using a commercial off-the-shelf throttle valve and a solid rocket motor case adapted for hybrid rocket testing. During throttled motor tests, the pressure ratio across the injector grows from a nominal value of 2.0 to greater than 3.0. This feature contrasts with the observed behavior of liquid rockets, where the injector pressure ratio drops significantly during deep throttle. This characteristic likely supports the observed hybrid burn stability during deep throttle. Data comparisons with a physics-based, throttled, hybrid rocket burn model accurately match for combustor pressure, thrust, and propellant consumption. At throttle levels approaching 20% of nominal, the N₂O exiting the throttle valve is entirely in a vapor state. The vapor chokes the injector and eliminates feed system coupling. This two-phase effect is another likely reason for the unexpected combustion stability observed at very deep-throttle levels. The ability to throttle deeply opens the possibility that hybrid thrusters could be simultaneously deployed for both main spacecraft propulsion and reaction control.

Nomenclature

A_{burn}	= fuel grain surface burn area, cm ²
$A_{c,\text{port}}$	= instantaneous mean cross-sectional area of fuel port, cm ²
A_{ev}	= throttle valve exit cross-sectional area, cm ²
A_{exit}	= nozzle exit area, cm ²
A_{ox}	= injector exit cross-sectional area, cm ²
A^*	= motor throat choking area, cm ²
a	= Saint Robert's burn parameter, cm/kPa ^{1/n}
$C_{d,\text{ox}}$	= injector discharge coefficient
C_p	= specific heat of combustion gases at edge of flame zone, J/kg · K
C_v	= valve flow coefficient
G	= oxidizer mass flux, kg/m ² · s
$h_{v,\text{solid fuel}}$	= specific enthalpy of gasification of solid fuel material, J/kg
I_{sp}	= specific impulse, s
L_{port}	= length of fuel port, cm
L^*	= ratio of chamber volume to choking area, m
\dot{m}_{fuel}	= fuel mass flow, kg/s
\dot{m}_{ox}	= oxidizer injector mass flow, kg/s
n	= hybrid rocket oxidizer mass flux exponent or solid rocket Saint Robert's burn exponent
O/F	= mean longitudinal oxidizer-to-fuel ratio
P_{ox}	= oxidizer injector upstream feed pressure, kPa
P_r	= Prandtl number of combustion gases at edge of flame zone
P_0	= combustion chamber pressure, kPa
R_g	= gas-specific constant, J/kg · K
\dot{r}	= fuel port linear regression rate, cm/s

$T_{\text{solid fuel}}$	= mean longitudinal solid fuel grain surface temperature, K
T_0	= combustor flame temperature, K
V_c	= combustion chamber volume, cm ³
X_1	= oxidizer feed line fluid quality
% MVT	= control valve servo position, percentage of maximum travel
γ	= ratio of specific heats or combustion products
μ	= viscosity of combustion gases at edge of flame zone, Pa · s
ρ	= fluid density, kg/m ³
ρ_L	= saturated fluid liquid density, kg/m ³
ρ_{ox}	= liquid oxidizer density, kg/m ³
$\rho_{\text{solid fuel}}$	= density of solid fuel material, kg/m ³
ρ_V	= saturated fluid vapor density, kg/m ³

I. Introduction

During the past 60 years, conventional launch systems have developed to a high state of capability; however, for a variety of reasons, these vehicles have become increasingly expensive to operate. Primary drivers for this increase in operating expense are safety and environmental regulations for dealing with hazardous and toxic materials. Although procedures are in place to allow hazardous and toxic propellants to be managed within tightly controlled government-operated test ranges, environmental restrictions associated with toxic propellant transport, storage, servicing, and clean up of accidental releases are rapidly making the use of hazardous propellants increasingly cost prohibitive. This growing regulatory burden has also significantly increased manufacturing complexity and has resulted in the requisite “support army” for flight operations. A recent study by the ESA's European Space Research and Technology Center has confirmed this assertion by identifying the essential element for achieving low-cost space access as “lowered production, operational, and transport costs due to reduced propellant toxicity and reduced explosion hazards” [1,2]. As a portion of space flight operations gradually shift from large defense contractors and government-run organizations to small commercial operations, these organizations will be willing to accept a slightly reduced system performance in exchange for a significant increase in overall system safety and “environmental friendliness.”

Presented as Paper 2012-4200 at the 48th AIAA/ASME/SAE/ASEE Joint Propulsion Conference & Exhibit, Atlanta, GA, 30 July–1 August 2012; received 22 February 2013; revision received 8 July 2013; accepted for publication 31 July 2013; published online 30 December 2013. Copyright © 2013 by Utah State University. Published by the American Institute of Aeronautics and Astronautics, Inc., with permission. Copies of this paper may be made for personal or internal use, on condition that the copier pay the \$10.00 per-copy fee to the Copyright Clearance Center, Inc., 222 Rosewood Drive, Danvers, MA 01923; include the code 1533-3876/13 and \$10.00 in correspondence with the CCC.

*Associate Professor, Mechanical and Aerospace Engineering Department, 4130 Old Main Hill/UMC 4130. Associate Fellow AIAA.

†Graduate Research Associate, Mechanical and Aerospace Engineering Department, 4130 Old Main Hill/UMC 4130. Student Member AIAA.

Hybrid rockets have the ability to fill this emerging gap in the commercial space market. Although it is generally acknowledged that hybrid rocket systems deliver lower performance and volumetric efficiency than conventional liquid- and solid-propelled rocket

systems, most commonly used hybrid rocket propellants are nontoxic and remain inert until purposely ignited in the combustion chamber. Thus, hybrid rockets present a significantly reduced potential for explosion and environmental contamination. Hybrid rocket systems are inherently safer and less expensive to manufacture, transport, service, and operate than conventional systems [3]. Because hybrid rocket fuel burn rates do not couple with the combustion chamber pressure, hybrid rockets exhibit a relative insusceptibility to grain flaws. Thus, hybrid rocket systems are also robust to aging issues that present a significant safety hazard for solid-propelled rocket systems. This capability for long-term storage has the potential to also significantly reduce overall operating costs.

Other advantages of hybrid rockets that can potentially offset lower performance levels include the capability for in-flight restart and throttle. Of particular interest is the ability for hybrid rockets to be deeply throttled while maintaining stable combustion. Traditionally, a deep-throttled rocket system has been defined as any system capable of a thrust “turndown” of 4:1 from its nominal thrust level. The ability to throttle deeply opens the possibility that hybrid thrusters can be simultaneously deployed for both main spacecraft propulsion and reaction control. Missile defense applications have also been proposed [4].

For liquid-propelled rockets, the upstream injector feed pressures and area ratios directly control the total mass flow, chamber pressure, and fuel oxidizer-to-fuel *O/F* ratio. Proper fuel and oxidizer atomization are critical for stable combustion [5]. Maintaining a sufficiently high-pressure drop across the injector for satisfactory atomization sets a practical lower limit to the depth of throttling that can be achieved by pressure modulation alone. Theoretically, a liquid rocket system can be throttled to any level by lowering the oxidizer and fuel feed pressures upstream of the injector. However, reducing propellant flow rates causes the upstream injector pressure to drop faster than the chamber pressure. At some point, the injector pressure ratio (IPR) becomes so low that coupling occurs between the chamber and propellant feed system.

As a rule of thumb, a pressure ratio of 1.25 or greater across the injector is required to insure proper combustion stability. This requirement limits the ability to throttle liquid rockets by using feed pressure only, typically 60–70% of the nominal operating thrust level. As a point of reference, the space shuttle main engine was normally throttled within a ratio of 1.67:1 [6].

Other factors also contribute to the complexity of deep-throttle liquid rocket systems. Both the fuel and oxidizer valves are required to precisely maintain near-optimal *O/F* ratios over a wide range of propellant mass flow rates. The combustor L^* (the ratio of chamber volume V_c to nozzle choking throat area A^*) is typically configured for a near-optimal *O/F* ratio. In a deeply throttled engine, small variations in either propellant flow rate can result in a significantly skewed *O/F* ratio, and this off-design condition can interact with the chamber L^* to produce either incomplete combustion or combustion instability. Either case will produce a suboptimal combustor performance compared with the full-throttle motor. Also, with the reduced propellant mass flow, turbopumps must also be designed to avoid cavitation, stalling, or surging. Turbomachinery components must have stable rotational and structural dynamics for a wide flow range. Regeneratively cooled liquid engines may also have insufficient heat transfer at high throttle turndown ratios.

Because of the aforementioned difficulties, deep-throttle liquid rocket engines nearly always require variable geometry injection systems. Injectors for deep-throttled liquid systems are generally based on the TRW pintle injector design [7]. The unique geometry and injection characteristics of the pintle injector distinguish it from injectors typically used on liquid-bipropellant rocket engines. The pintle injector features a coaxial flow stream where one propellant (either fuel or oxidizer) flows through an outer tube and exits as a cylindrical stream. The complementary propellant flows through an inner tube and impinges on a pintle-shaped poppet valve similar to a garden hose nozzle. The pintle causes the inner propellant to spray outward in a broad cone that impinges on the outer flow stream. Pintle-style rocket injectors feature complex internal geometries and are all “custom builds.” Commercial off-the-shelf (COTS) pintle

injectors are generally not available for rocket systems. Each design must be tuned to the specific combustor to achieve proper combustion properties.

The Apollo program lunar descent engine employed a TRW-designed pintle injector and was capable of a 10:1 turndown ratio [8]. An Aerojet/Roxel team has recently demonstrated a pintle injector engine with a 20:1 turndown ratio for the U.S. Navy’s Joint Common Missile program [9]. A Pratt and Whitney Rocketdyne team has recently modified the injection system on an existing RL-10 rocket engine to achieve turndown ratios of 13:1 and 17.6:1 [10].

Much of the throttling technology developed for liquid-propelled rockets is applicable to hybrid rockets. There is, however, one major exception. When a liquid rocket is throttled, both the oxidizer and fuel mass flow rates can be directly controlled using both the upstream feed pressure and injector flow area. In contrast, when a hybrid motor is throttled, only oxidizer mass flow rate is directly controlled and the fuel mass flow rate is an indirect response to the change in oxidizer mass flow. The fuel mass flow rate is driven primarily by the rate of fuel pyrolysis and the continuously variable fuel port surface burn area [11]. Thus, to precisely understand the hybrid throttling phenomena, a working model of influence of oxidizer mass flow and fuel port geometry upon fuel pyrolysis and the resulting linear regression rate is necessary.

Hybrid motor fuel burn characteristics are distinctly different from those of solid-propellant rockets. In a solid-propellant system, the oxidizer and fuel components are homogeneously mixed during manufacturing, and the burn properties including fuel regression rate and *O/F* ratio are fixed by the a priori propellant formulation and fuel port geometry. Combustion results from chemical reactions at the propellant surface, and combustion pressure directly drives the rate of reaction. Thus, the regression rate couples directly with the combustor chamber pressure by the well-known Saint Robert’s Law [12]:

$$\dot{r} = a \cdot P_0^n \quad (1)$$

In Eq. (1), \dot{r} is the mean linear rate of regression and P_0 is the combustion chamber pressure. The empirical parameters $\{a, n\}$ are a function of the propellant formulation and fuel grain temperature. Because the propellant gasification rate in a solid rocket motor is a strong function of the chamber pressure, solid-propelled rockets cannot be deeply throttled in any practical sense. As the chamber pressure drops, the rate of fuel gasification also drops, and combustion is quickly extinguished.

Conversely, the fuel regression rate of hybrid rocket systems does not couple with the combustor chamber pressure. Complex heat transfer and transport phenomena within the flame zone and boundary layer drive the rate of fuel pyrolysis. Boundary-layer mixing creates a region where oxidizer flow from the center of the motor combustion port mixes with vaporized gases leaving the fuel wall. The flame zone where the combustion of fuel and oxidizer primarily takes place lies close to the fuel wall. Heat transfer from the flame zone to the solid surface drives the fuel pyrolysis rate [13]. The average rate at which the fuel burns perpendicular to the longitudinal axis of the motor is referred to as the “mean longitudinal regression rate.”

Marxman and Gilbert demonstrated that hybrid rocket fuel regression rates are dominated by thermal diffusion and transport mechanisms and not chemical reactions [14]. Thus, Saint Robert’s law is not applicable for predicting the fuel regression rate. Saint Robert’s law was modified to calculate fuel regression rate as a function of the oxidizer mass flux:

$$\dot{r} = a \cdot G^n \quad (2)$$

In Eq. (2), G is the oxidizer mass flux and the parameters $\{a, n\}$ are empirically determined. Marxman et al. [15] later added modifications to account for “radial blowing” caused by the ablating fuel grain. Changes based upon radiant heat transfer to the fuel surface were also proposed but were found to be negligible for hybrid rocket fuels free of metallic particles. Later studies performed by Strand et al. [16] and later Chiaverini et al. [17] modified the experimental coefficients derived by Marxman and Gilbert [14] to

better agree with a wider set of hybrid motor regression rate data. The original Marxman and Gilbert model predicts the fuel regression rate in terms of the surface skin friction and surface-blowing coefficient. The model does not sufficiently close to allow physics-based calculations using a priori definitions for the motor geometry, oxidizer feed pressure, and propellant selection.

Eilers and Whitmore have developed a useful closed-form regression rate model using the enthalpy balance between the fuel grain surface and a turbulent flat-plate boundary layer [18]. The form of the model is similar to Marxman and Gilbert's original model [14], but allows physics-based calculations of the longitudinally averaged fuel regression rate based on the instantaneous oxidizer mass flux:

$$\dot{r} = \left(\frac{0.047}{\rho_{\text{solid fuel}} \cdot P_r^{2/3}} \right) \cdot \left(\frac{\mu}{L_{\text{port}}} \right)^{1/5} \cdot \left(\frac{C_p \cdot (T_0 - T_{\text{solid fuel}})}{h_{v_{\text{solid fuel}}}} \right)^{0.23} \left(\frac{\dot{m}_{\text{ox}}}{A_{c_{\text{port}}}} \right)^{4/5} \quad (3)$$

In Eq. (3), the parameters L_{port} and $A_{c_{\text{port}}}$ are the port length and instantaneous cross-sectional area; $\rho_{\text{solid fuel}}$, $h_{v_{\text{solid fuel}}}$, and $T_{\text{solid fuel}}$ are the density, specific enthalpy of gasification, and mean longitudinal surface temperature of the solid fuel grain material; and \dot{m}_{ox} is the oxidizer mass flow. The parameters μ , C_p , P_r , and T_0 are the viscosity, specific heat, Prandtl number, and flame temperature of the gaseous combustion byproducts. For the regression model of Eq. (3), these parameters are typically calculated based on the total oxidizer-to-fuel ratio and mean combustion chamber pressure and assuming equilibrium combustion chemistry. Clearly, the term $\dot{m}_{\text{ox}}/A_{c_{\text{port}}}$ is the mean longitudinal mass flux, and the "Marxman" exponent for this model is $n = 4/5$. Equation (2) was evaluated for several fuel grain materials and multiple fuel port geometries and was found to accurately predict the mean longitudinal regression rate [19,20].

Equation (1) clearly demonstrates that the fuel regression rate will drop rapidly as the motor burns, the fuel port opens up, and the cross-sectional area grows. This regression rate decrease has a significant effect on the O/F ratio. Equation (1) can be used to describe the time evolution of the O/F ratio by examining the total fuel mass flow rate, calculated as

$$\dot{m}_{\text{fuel}} = \rho_{\text{solid fuel}} \cdot A_{\text{burn}} \cdot \dot{r} \quad (4)$$

In Eq. (4), A_{burn} is the total surface burn area in the fuel port. The instantaneous O/F ratio is calculated by

$$O/F = \frac{\dot{m}_{\text{ox}}}{\rho_{\text{solid fuel}} \cdot A_{\text{burn}} \cdot \dot{r}} = \frac{\dot{m}_{\text{ox}}}{\rho_{\text{solid fuel}} \cdot A_{\text{burn}} \cdot (0.047/(\rho_{\text{solid fuel}} \cdot P_r^{2/3})) \cdot (\mu/L_{\text{port}})^{1/5} \cdot (C_p \cdot (T_0 - T_{\text{solid fuel}})/h_{v_{\text{solid fuel}}})^{0.23} (\dot{m}_{\text{ox}}/A_{c_{\text{port}}})^{4/5}} \quad (5)$$

Collecting terms, Eq. (5) is rewritten as

$$O/F = \frac{(\dot{m}_{\text{ox}})^{0.5} \cdot (A_{c_{\text{port}}}/A_{\text{burn}})^{4/5}}{(0.047/\rho_{\text{solid fuel}} \cdot P_r^{2/3}) \cdot [A_{\text{burn}}(\mu/L_{\text{port}})]^{1/5} \cdot (C_p \cdot (T_0 - T_{\text{solid fuel}})/h_{v_{\text{solid fuel}}})^{0.23}} \quad (6)$$

For a cylindrical fuel port, Eq. (6) can be reduced to

$$O/F = 21.2766 \cdot P_r^{2/3} \cdot \left(\frac{h_{v_{\text{solid fuel}}}}{C_p \cdot (T_0 - T_{\text{solid fuel}})} \right)^{0.23} \cdot \left(\frac{\dot{m}_{\text{ox}}}{\pi \cdot \mu \cdot L_{\text{port}}^2} \right) \cdot D_{\text{port}}^{3/5} \quad (7)$$

For a constant oxidizer mass flow as the motor burns and the mean effective fuel port diameter grows, the O/F ratio grows without

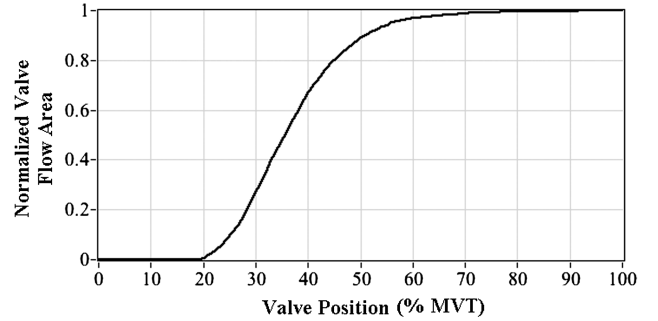


Fig. 1 Normalized throttle valve flow area as function of maximum valve travel.

bound. This effect results in an increasingly "leaner" combustion mixture that burns significantly hotter and may lead to combustion instability, erosive burning, or nozzle erosion near the end of a long duration motor burn. To prevent problems caused by extremely lean combustion mixtures, Eqs. (6) and (7) may be used to size the various motor components so that the motor burn starts out significantly fuel rich and ends at an O/F ratio that will not cause motor instability or erosion problems.

Fortunately, the effect of throttling the hybrid motor by reducing the oxidizer mass flow can in part compensate for the rising O/F ratio as a function of burn time. This fortunate compensating effect makes hybrid rockets significantly less susceptible to combustion instabilities during throttling than liquid-propelled systems. If the throttling schedule is prescribed judiciously, it should be possible to throttle a hybrid system very deeply without the stability issues associated with liquid rockets.

II. Hybrid Rocket Deep-Throttle Verification Experiment Test Apparatus

This section describes test apparatus and procedures for a deep throttling experiment designed to verify the hypothesis presented in the preceding section. The experimental apparatus was constructed using mostly COTS hardware and was ultimately designed to demonstrate the limits of throttling for a medium-scale nitrous oxide (N_2O) and hydroxyl-terminated polybutadiene (HTPB) hybrid rocket motor. All throttling experiments were performed in the Utah

State University Propulsion Research Laboratory's on-campus test cell using existing support infrastructure and instrumentation. Peterson et al. [21] present detailed descriptions of this test infrastructure including the oxidizer management system, data acquisition and automation hardware, and test instrumentation. Minor modifications, including installation of the throttle actuation and control system, were required for the deep-throttle tests. This section will describe the throttle actuation and control system and its interface to the hybrid motor used for the throttling tests.

Table 1 Motor case, nozzle, injector, and fuel grain dimensions

Items	Dimensions
Motor case	70.2 cm length 98 mm diam
Nozzle	2.21 cm ² , throat area (1.64 cm diam) 9.27 cm ² exit area (3.44 cm diam)
Injector	4.2 expansion ratio 0.115 cm ² exit area (0.383 cm diam), A_{ox} 0.40 discharge coefficient, $C_{d_{ox}}$
Fuel grain	57.15 cm length 82.6 mm diam 5.07 cm ² port area

A. Throttle Actuation System

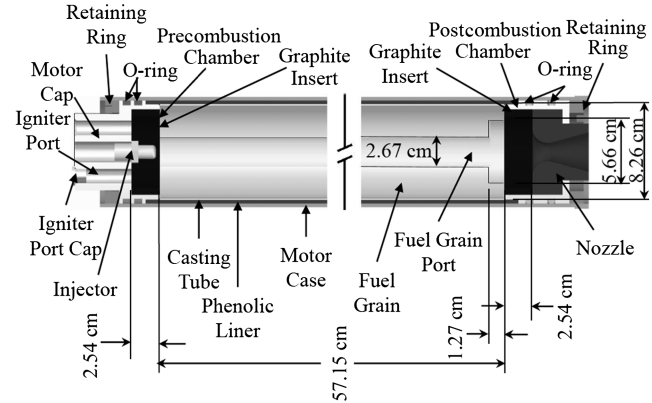
The throttle valve was selected following an extensive trade study that considered 1) range of control authority, 2) weight, 3) cost, 4) commercial availability, and 5) linearity of flow profile. Ultimately, a McMaster-Carr[‡] one-half in. stainless-steel circular ball valve with a 5/16 in. port was selected for this experiment. This inexpensive industrial valve was not rated for aerospace applications and was certified for this test through a series of cold-flow and nonthrottled hot-flow motor tests [21]. An industrial valve was selected over a custom pintle valve mostly as a time- and cost-saving measure. The ball valve also offers a higher response rate.

For the selected valve, the flow coefficient $C_v = 0.70$ ensured that the flow would not cavitate across the fully open valve at the nominal mass flow of 310 g/s when the nitrous oxide feed pressure was held at approximately 400 kPa (58 psia) above the saturation pressure. This “no-cavitation” design restriction allowed for more consistent run-to-run burn profiles for the unthrottled motor. Figure 1 plots the normalized valve flow area as a function of the percentage of maximum travel (% MVT). The valve remains essentially closed until 20% MVT, changes linearly between 20 and 50% MVT, and then rapidly loses response authority as the valve approaches 100% open. If one were trying to precisely throttle in the 85–100% throttle region, this nonlinear profile with diminishing control authority near the full-open point would normally present problem. However, because the objective of this experiment is to demonstrate deep throttle, this valve area profile was deemed acceptable.

The selected actuator for the throttle system was an Invenscience LC Torxis Servo i00600 rotary servomotor[§] with a built-in Pololu jrk 21v3 position controller.[¶] A custom mounting bracket and linkage were designed to attach the servo to the valve. The servo is controlled by a 0–5 V dc proportional analog command that corresponds to the 0–100% MVT full range of rotation for the throttle valve. The servo produces 11.3 N · m of continuous torque and 22.6 N · m of peak torque with a peak current draw of 3 A. The peak torque output is more than four times the calculated static opening torque of the valve at the oxidizer feed pressure, approximately 5400 kPa (780 psia), and assures the valve will not stall during throttling, and valve damping will not hinder the speed of the controller.

B. Test Motor

The throttling tests used a well-known motor configuration that had been previously tested and characterized before the insertion of the throttling valve. Data from these early tests served as a baseline for the throttling experiment. The previous tests demonstrated that the oxidizer delivery system with a 5520 kPa (800 psia) regulated top pressure delivered a nominal oxidizer mass flow of approximately 310 g/s, with a mean nominal thrust level near 800 N (180 lbf) [19]. The early baseline tests used both HTPB and acrylonitrile butadiene

**Fig. 2 Schematic of 98 mm hybrid test motor.**

as fuel grain materials. Table 1 summarizes key geometric parameters of the baseline motor configuration.

For this test configuration, a commercially available Cesaroni® 98 mm solid rocket motor^{**} was modified to replace the original motor cap and nozzle ring with custom-designed parts compatible with hybrid rocket testing. Figure 2 presents a schematic of the test motor. This configuration offers a ready-made flight-weight configuration and allows rapid reload between motor tests. To reduce run-to-run variability caused by nozzle erosion, nozzles fabricated from a single piece of high-density graphite replaced the original manufacturer-supplied high-erosion phenolic nozzle. Two Estes “mini A class” 10 g solid rocket motors,^{††} ignited by electronic matches, were inserted into the injector cap to initiate the motor combustion.

As mentioned previously, the throttling tests used HTPB as the fuel grain material. The HTPB fuel grains were mixed, cast, and degassed by the test team at Utah State University using industry standard fabrication practices. The cylindrical-port fuel grain was fabricated to fit snugly into the motor case described in the preceding section. A postcombustion chamber was premanufactured into the fuel grain. Each fuel grain was approximately 57.15 cm in length, 8.26 cm in diameter, the initial fuel port diameter was 2.54 cm, and postcombustion chambers were 5.66 cm in diameter and 1.27 cm deep. Each HTPB fuel grain weighed approximately 2.62 kg (5.76 lbm). The fuel grain is bonded into a cardboard sleeve using high-temperature silicone adhesive. This sleeve is inserted into a phenolic insulating liner, and then into the aluminum motor casing. The nozzle and motor cap assemblies are sealed with O-rings. The aluminum motor case acts as the pressure vessel for the motor.

The single spray nozzle injector port was designed to protrude approximately 1 cm into the top of the fuel grain to eliminate impingement erosion on the upper fuel section and reduce the chances of initiating chaotic or unpredictable burning along the length of the motor. The injector characterization tests assumed an incompressible fluid flow; consequently, because of the nitrous oxide transition from liquid to vapor as it enters the injector port and exits into the combustion chamber, the injector discharge coefficient has an unusually low value, $C_{d_{inj}} = 0.40$.

III. Results and Discussion

This section presents results from the throttle testing campaign. Results from the deep-throttle test are presented and compared with predictions from the hybrid motor combustion model previously developed by Eilers and Whitmore [18]. The model comparisons act as an aid in interpreting the results of the deep-throttle test. Two-phase effects from the nitrous oxide flow through the throttling valve are identified and quantified.

[‡]McMaster-Carr Item 45395K105; data available online at <http://www.mcmaster.com/#catalog/118/433/-i4e9p2v>.

[§]Data available online at http://www.invenscience.com/index_les/Page923.htm [retrieved 8 July 2013].

[¶]Data available online at <http://www.pololu.com/catalog/product/1392> [retrieved 8 July 2013].

^{**}Data available online at www.pro38.com/products/pro98/pro98.php [retrieved 8 July 2013].

^{††}Data available online at http://www.hobbylinc.com/estes_a_model_rocket_engines.

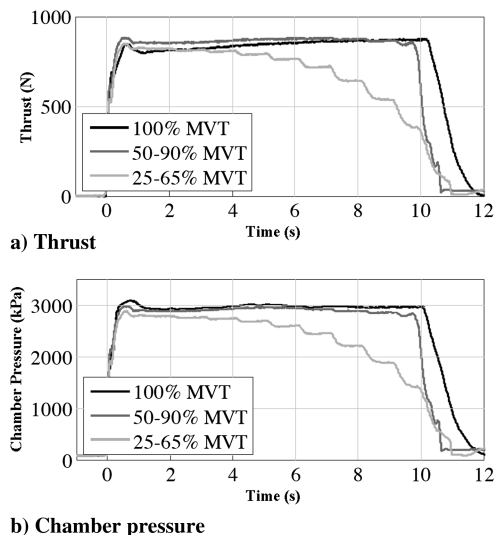


Fig. 3 Thrust and chamber pressure from initial throttle tests with hybrid systems.

A. Initial Throttle-Evaluation Test Results

Before performing the deep-throttle tests, a series of three hot-fire tests were performed to demonstrate the effectiveness of the throttle actuation system at moderate throttle levels. Figure 3 shows the thrust and chamber pressure time histories obtained during these initial tests. During the first test, the throttle valve was left completely open throughout the duration of the burn. For the second test, the throttling valve started at 90% MVT and closed in steps of 5% MVT every second to 50% MVT. The third test began at the 65% MVT position and was again closed 5% MVT every second until finishing at the 25% MVT position.

The thrust and chamber pressure levels obtained from the test with the fully open throttle valve agree well with the previously collected data for this motor [19], indicating that the fully open-throttle port did not produce a significant pressure loss or oxidizer mass flow restriction. Results from the two throttled tests demonstrated, within the linear control range (from 50 to 20% MVT), the control authority was quite precise. At the upper end of the valve range (from 100 to 60% MVT), there was significantly reduced control authority. For all three tests, good flame stability was observed and feed system coupled (nonacoustic) combustion instability [22] modes were absent for all throttle levels. These results gave the team confidence to proceed with the deep-throttle tests.

B. Deep-Throttle Test Results

Because the ball valve was found to be less effective from approximately 100 to 60% MVT, for the deep-throttle tests, the first valve motor increment would move from 100 to 50% MVT. Figure 4 shows the prescribed valve position, scheduled as a function of time. As the throttle approached the minimum area valve, the valve

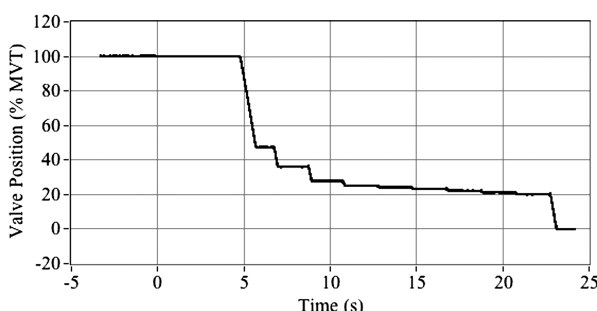


Fig. 4 Prescribed throttle valve position schedule.

position increments were successively reduced to allow correspondingly greater throttle precision.

Figure 5 presents the measured thrust and chamber pressure time histories for the deep-throttle test, surrounded by video still images corresponding to several of the thrust set points. The indices displayed in the images are the calculated percentage of peak thrust and a time stamp corresponding to the location on the time axis of the plot. These indices are also displayed along the time history trace of the thrust plot. During this test, a bright-orange-to-white flame was observed until approximately 15 s into the burn when the motor flame became increasingly "sooty." Approaching 20 s from ignition, the motor began to "chug" loudly, and approximately 3 s later, combustion ceased. The thrust and chamber time history plots indicate that the thrust was well controlled and combustion was stable for very low throttle levels, approximately 1.5% of the nominal thrust level.

Figure 6 plots the corresponding power spectra for three time segments of the chamber pressure time history: 1) data from the first 8 s of the record, 2) data from the next 10 s of the record, and 3) data from the final 4 s of the record. The power spectra calculated using the first two time segments are nearly identical and show no low-frequency nonacoustical or high-frequency acoustical modes. The spectra for time segments 1 and 2 exhibit a log-linear decay and are indicative of a classic turbulent-eddy transport process [23]. In contrast, the power spectrum calculated using the final 4 s of the data record does not display the classical log-linear decay. The spectrum is relatively flat below 10 Hz and then exhibits a large mode between 16 and 20 Hz. These pressure oscillations for this frequency band are clearly visible in Fig. 6a. At point 3 in the test, it appears that, instead of energy being distributed primarily in the larger flow eddies, the energy concentrates within a narrow frequency band, and this energy concentration excites the nonacoustical combustion instability modes.

Significantly, before the instability point is reached, the thrust level is approximately 12 N. This thrust level represents a turndown ratio of 67:1. This 67:1 turndown was accomplished using an inexpensive COTS ball valve and a single-port spray nozzle injector, with each component costing less than \$50. To the authors' knowledge, this event marks the lowest stable turndown ever achieved on a hybrid- or liquid-propelled rocket motor.

C. Effect of Throttle Valve on Nitrous Oxide Fluid Phase

As described previously, the run tank was pressurized at approximately 350–400 kPa above N₂O vapor pressure to assure that the oxidizer flow is entirely supersaturated liquid when entering the throttle valve. The throttle valve was sized to ensure that the full-open pressure drop was insufficient to allow the liquid to drop below the supersaturated condition until it reached the injector port. However, once the throttle valve begins to close, there is a significant drop in the flow coefficient, and the pressure drop brings the liquid to a saturated condition. The data presented by Fig. 7 demonstrate this occurrence. Figure 7a plots the measured run tank pressure, the measured pressure just downstream of the throttle valve, and the vapor pressure at the measured fluid temperature downstream of the run valve. Figure 7b plots the sensed temperature immediately downstream of the throttle valve and ahead of the motor injector. In the full-open condition, there is very little pressure loss between the run tank and the throttle valve. However, soon after the throttling begins, the pressure drops sufficiently to allow the fluid to reach saturation state, approximately 6 s after the beginning of the test.

The Helmholtz free energy model developed by Span and Wagner [24,25] was used to calculate the fluid density ρ leaving the throttle valve based on the measured temperature and pressure. Using this density value and the saturation densities for the vapor ρ_V and liquid ρ_L phase of the nitrous oxide at the fluid exit temperature, the fluid quality χ was calculated by Eq. (8) [26]:

$$\chi = \frac{\rho_v}{\rho} \left(\frac{\rho_l - \rho}{\rho_l - \rho_v} \right) \quad (8)$$

Figure 8 plots the density time history and the calculated fluid quality as a function of the throttle valve position in % MVT. Before the first

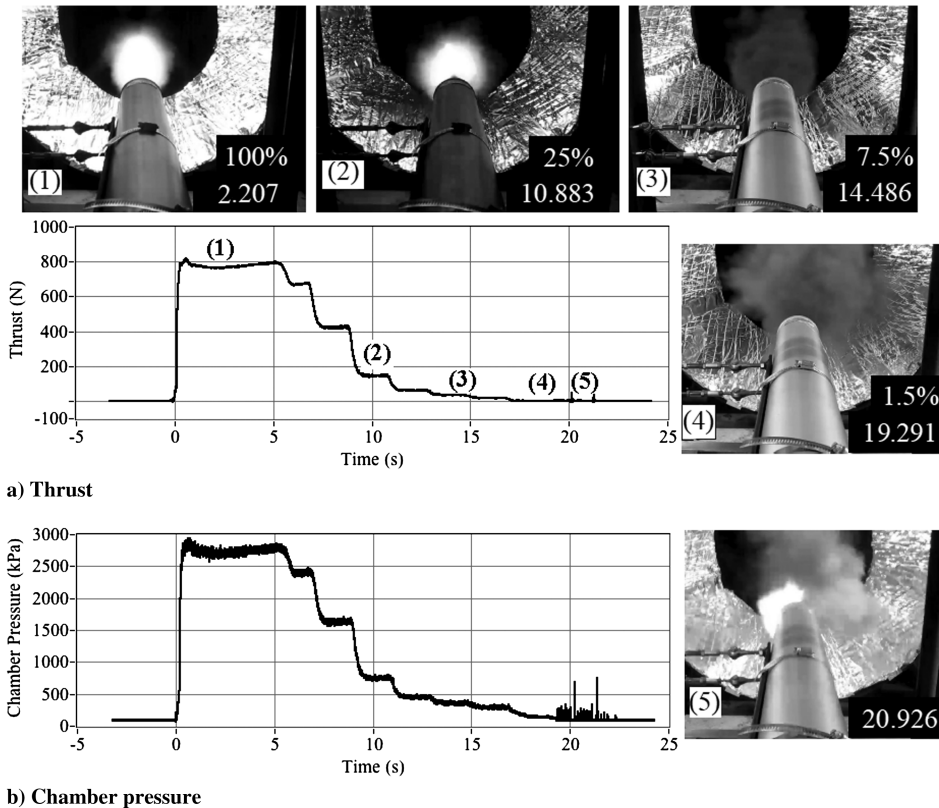
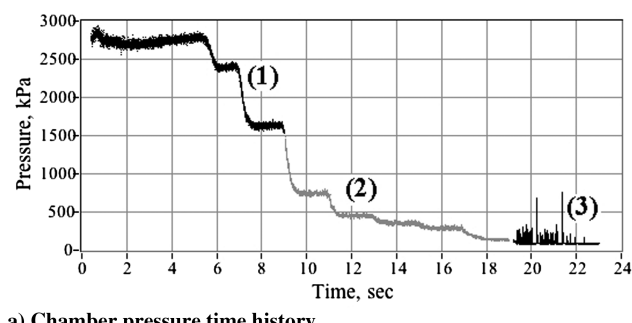
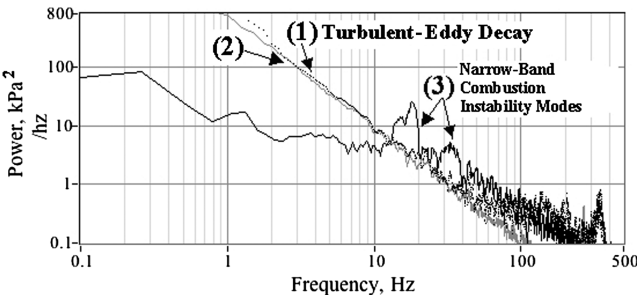


Fig. 5 Thrust time history profile with video stills from deep-throttle test.



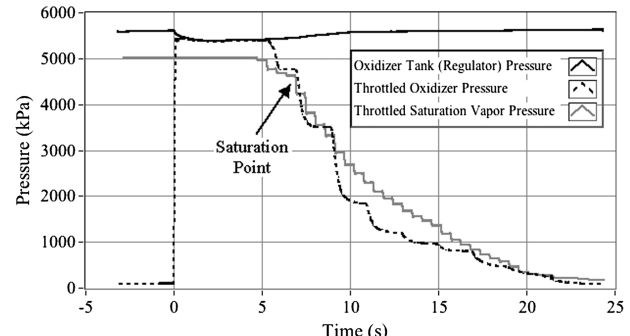
a) Chamber pressure time history



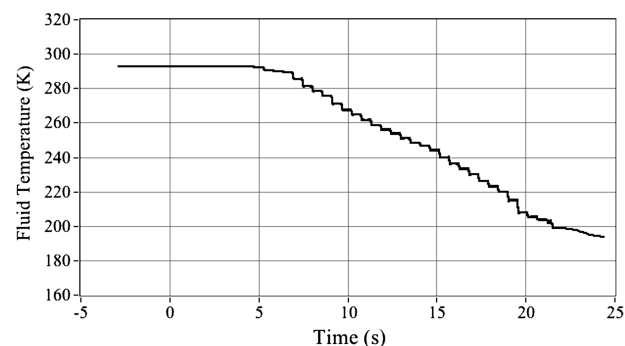
b) Chamber pressure power spectrum

Fig. 6 Power spectra of deep-throttle chamber pressure time history segments.

major throttle step, the fluid is clearly in a supersaturated liquid state. Between the first and third throttle steps down, corresponding to throttle position 50–25% MVT, the fluid varies between a liquid and vapor, and as the throttle approaches the 20% MVT setting, the fluid state is entirely vapor. The throttle valve effectively throttles the oxidizer mass flow by reducing the inlet flow area and reducing the fluid density. This change in fluid state is a likely reason for the unexpected high level of combustion stability observed at very low



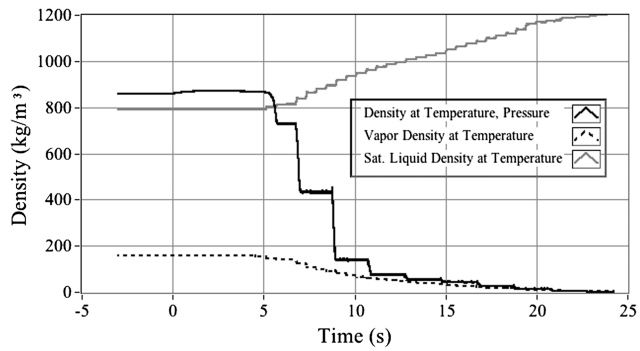
a) Tank pressure, Throttle valve exit pressure, Saturation vapor pressure



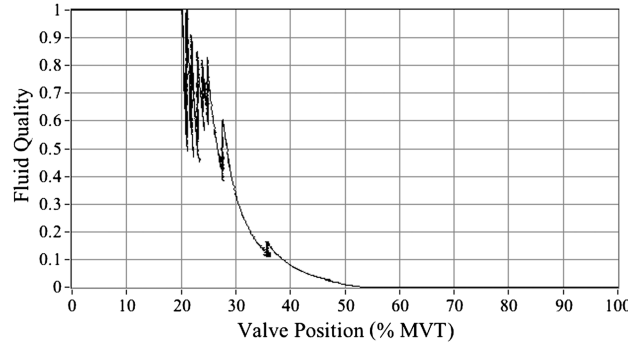
b) Throttle valve fluid temperature

Fig. 7 Run tank pressure, throttled valve pressure, saturation pressure, and run valve fluid temperature comparison.

throttle levels. At these low feed pressure levels, because the nitrous oxide is entirely vapor, the injector is likely choked and feed system coupling is effectively eliminated. The instability observed in Fig. 6 likely occurs once the oxidizer mass flow drops so low that the injector is no longer choked and feed system coupling can occur.



a) Density



b) Fluid quality

Fig. 8 Variation of nitrous oxide fluid density and quality during motor throttle.

D. Numerical Model Comparison

As a final step to understanding the motor behavior observed during the deep-throttle test, the motor data are compared with the hybrid rocket simulation previously developed and verified by Eilers and Whitmore [18] and Peterson et al. [21]. This model uses the regression model previously stated in Eq. (2), with postcombustion gas properties calculated using the NASA standard code “Chemical Equilibrium with Applications” [27]. Assuming the nozzle throat chokes immediately, a balance between the gases coming into the fuel port and the gases leaving through the choked throat determines the time response of this chamber pressure growth. Here the time evolution of the chamber pressure is calculated as

$$\frac{\partial P_0}{\partial t} = \frac{A_{\text{burn}} \dot{r}}{V_c} [\rho_{\text{fuel}} R_g T_0 - P_0] - P_0 \left[\frac{A^*}{V_c} \sqrt{\gamma R_g T_0 \left(\frac{2}{\gamma+1} \right)^{[(\gamma+1)/(\gamma-1)]}} \right] + \frac{R_g T_0}{V_c} A_{\text{ox}} C_{d_{\text{ox}}} \sqrt{2\rho_{\text{ox}}(P_{\text{ox}} - P_0)} \quad (9)$$

The oxidizer mass flow rate is modeled by the incompressible discharge coefficient formula

$$\dot{m}_{\text{ox}} = A_{\text{ox}} C_{d_{\text{ox}}} \cdot \sqrt{2 \cdot (\rho_{\text{ox}} - P_0)} \quad (10)$$

In Eqs. (9) and (10), R_g and γ are the gas constant and ratio of specific heats for the combustion by products, A_{ox} and $C_{d_{\text{ox}}}$ are the oxidizer injector port area and discharge coefficient, and ρ_{ox} and P_{ox} are the fluid density and pressure entering the upstream side of the injector. The motor exit mass flow and thrust are calculated using the standard one-dimensional De Laval nozzle flow equations [28].

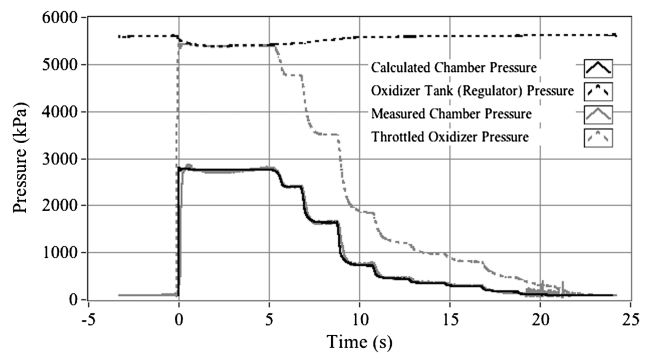
For the unthrottled motor, Eq. (10) is reasonably accurate provided the motor is burned using a “top pressure” higher than the saturation pressure of the N_2O . The throttling effect, with the resulting two-phase flow, clearly complicates this calculation. Dyer et al. [29] have developed a two-phase nonhomogeneous, nonequilibrium (NHNE) model for fixed geometry ports, and this model was demonstrated as

accurate by Whitmore and Chandler [26]. Peterson et al. [30] successfully applied the NHNE method to hybrid motors throttled to 50% of full thrust.

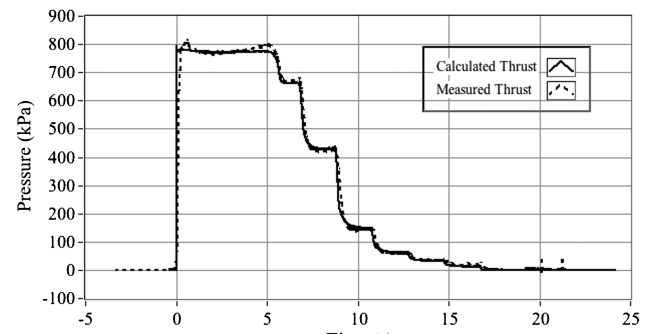
Unfortunately, when the motor is deeply throttled, the model does not account for the nearly all-vapor state of the oxidizer entering the injector and becomes inaccurate when the entering fluid quality rises above the 0.6–0.7 range. Instead, for this calculation, the measured pressure downstream of the throttle valve (Fig. 7) and density calculated using the pressure and temperature downstream of the throttle valve (Fig. 8) are used as the P_{ox} and ρ_{ox} inputs to Eqs. (9) and (10). Figure 9 presents comparisons for the calculated and measured chamber pressure and thrust time histories. Using the measured feed pressure and calculated density as inputs, the model very accurately captures the features of the deep-throttle test.

Figure 10 plots the calculated O/F ratio and IPR time histories. Figure 10a compares the O/F ratio for the throttled motor against the expected O/F ratio for the unthrottled motor. Figure 10b compares the calculated pressure ratio across the injector P_{ox}/P_0 to the measured value. As expected, the unthrottled motor O/F ratio continues to grow throughout the burn, whereas the throttled motor O/F ratio drops once the throttling process has begun. This calculation supports the assertion made earlier in the Introduction of this paper. For the unthrottled motor, a long burn will result in high O/F ratio and will produce significant nozzle and perhaps injector erosion. Instead of a decreasing IPR, as would be expected for a throttled liquid system, in the hybrid motor, the IPR actually grows during the throttle and is likely another characteristic that supports the burn stability during the deep throttle.

Finally, Fig. 11 compares the calculated and measured total propellant consumption and the mean specific impulse. Figure 11a compares the model predictions for consumed oxidizer and fuel mass against the measured values. The consumed oxidizer mass was measured directly using the load cells that support the run tank. There was no direct measurement of the fuel consumption during the tests and the plotted value is fuel grain mass loss measured after the test was completed. The model agreements for both oxidizer and fuel mass consumption are excellent, indicating that both the regression rate model and the injector flow model are accurate. Figure 11a

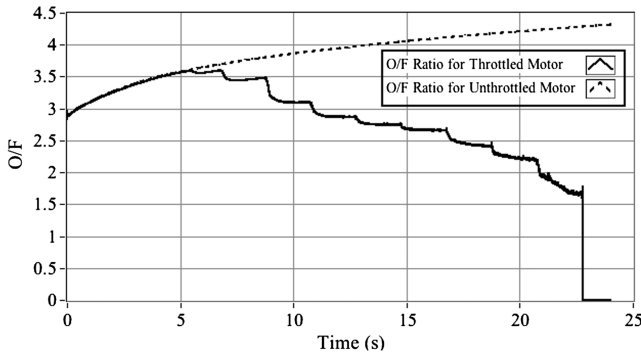


a) Oxidizer feed pressure and chamber pressure

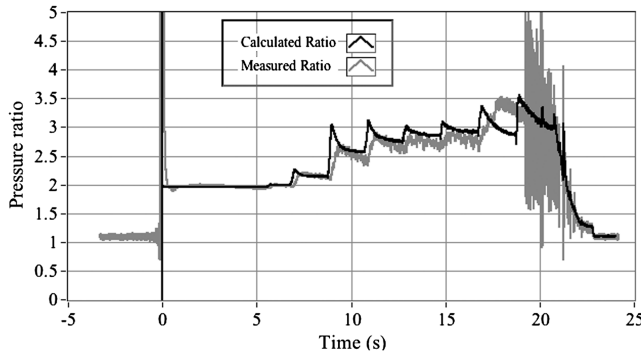


b) Thrust

Fig. 9 Model comparisons for chamber pressure and thrust for deep-throttle test.

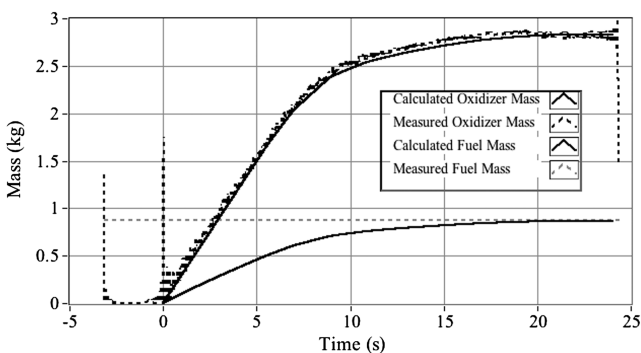


a) Oxidizer-to-Fuel mass flow ratio

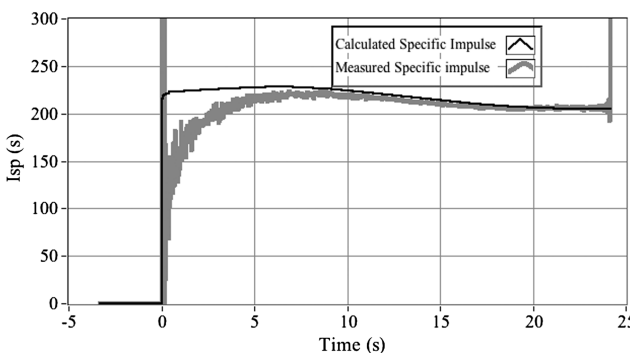


b) Injector pressure ratio

Fig. 10 Model comparisons for oxidizer-to-fuel ratio and injector pressure ratio.



a) Consumed oxidizer and fuel mass comparisons



b) Specific impulse

Fig. 11 Model comparisons for consumed propellant and mean specific impulse.

compares the mean I_{sp} calculated as the accumulated impulse divided by the consumed propellant mass at each point in the time history. Because there was no accumulated fuel consumption measurement in this test, the sum of the calculated fuel consumption and measured oxidizer consumption were used to calculate the “measured” I_{sp}

value. Once throttling begins, there is a moderate “tail off” in I_{sp} . At the deep-throttle levels, the exit pressures become quite low, and the nozzle is significantly overexpanded at the test ambient pressure conditions (86 kPa). This effect certainly contributes to the I_{sp} tail off. Other factors, such as lowering O/F ratio as the motor is throttled (Fig. 10) also likely contribute to the performance decrease. The total impulse method for calculating the I_{sp} , where the startup and burnout transients are included in the calculation, contributes the relatively low overall I_{sp} values for this motor.

E. Proposed Follow-Up Research

Because of budgetary and programmatic restrictions, the deep-throttle tests have not been repeated at this point. Soon after the completion of the deep-throttle test presented in this paper, the test apparatus was employed to perform a series of successful tests in which the throttle loop was successfully closed using both thrust and chamber pressure as feedbacks. Peterson et al. present those detailed results [30]. It is highly desirable that the deep-throttle tests be repeated to establish a statistical database for the system performance. Now that the deep-throttle combustion model has been verified, the model will be employed to develop a throttle schedule that produces a more consistent O/F ratio as the fuel grain burns. Clearly, through a series of iterative tests, it would be possible to develop a nearly flat O/F ratio for the throttled motor. Also, now that the limits of throttle stability are known, follow-up tests will attempt to ramp back up to full throttle once a very high turndown ratio has been achieved. Throttling experiments using a custom-built pintle control valve are highly desirable, but are beyond the scope of the currently funded budget for this project.

IV. Conclusions

Because of their inherent design safety, hybrid rocket systems that employ nontoxic, nonexplosive propellants have the potential to fulfill a substantial role in the emerging commercial space market and other defense applications. Although hybrid systems generally deliver lower specific impulse I_{sp} than conventional bipropellant liquid rockets and lower volumetric efficiency than solid rockets of the same thrust level, advantages that can offset the lower performance level include the capability for in-flight restart and a wide throttle range. The ability to throttle deeply opens the possibility that hybrid thrusters can be simultaneously deployed for both main spacecraft propulsion and reaction control.

This research project has investigated the potential to deeply throttle a hybrid rocket motor. Analysis presented in this paper conclude that the effect of throttling the hybrid motor by reducing the oxidizer mass flow can in part compensate for the normally occurring rise in oxidizer-to-fuel ratio as the motor burns and the fuel port opens up. This fortunate compensating effect makes hybrid rockets significantly less susceptible to combustion instabilities during throttling than liquid-propelled systems. Deep throttle using pressure regulation alone should be possible.

An experiment to test this hypothesis is proposed. Results from a deep-throttle test of a medium-scale hybrid rocket motor that uses nitrous oxide and hydroxyl-terminated polybutadiene as propellants are presented. Details of the experimental apparatus, including 1) the oxidizer delivery and management system, 2) the throttle actuation and control system, 3) data acquisition and automation hardware, 4) test instrumentation, and 5) the test motor, are presented.

The motor was successfully throttled from a nominal thrust level of 800 to approximately 12 N before encountering any combustion instability. During the throttled motor tests, the pressure ratio across the injector grows from a nominal value of 2.0 to greater than 3.0. This motor feature likely supports the burn stability during deep throttle and is in contrast to the rapidly lowered injector pressure ratio during deep throttle of liquid rocket systems. The test data also demonstrate that, as the test hybrid throttle level approached 20% of the nominal thrust level, the nitrous oxide exiting the throttle valve and entering the injector is entirely in a vapor state. The nitrous oxide vapor chokes the injector and effectively eliminates any feed system coupling. This two-phase choking effect is another likely reason for

the unexpected combustion stability observed at very deep-throttle levels.

The observed turndown ratio of 67:1, accomplished using an inexpensive hardware is a significant accomplishment. By comparison, the space shuttle main engine was normally throttled within a ratio of 1.67:1. Turndown ratios on liquid rockets with variable-geometry injectors have approached 20:1. To the authors' knowledge, this event marks the lowest stable turndown ever achieved on a hybrid-, solid-, or liquid-propelled rocket system.

Acknowledgments

The authors of this paper thank the Space Dynamics Laboratory of North Logan, Utah for their partial funding of this project through their Independent Research and Development program. The authors also thank the intellectual property services office at the Utah State University Research Foundation for filing the patent disclosures on this work.

References

- [1] Haeseler, D., Bombelli, V., Vuillermoz, P., Lo, R., Marée, T., and Caramelli, F., "Green Propellant Propulsion Concepts for Space Transportation and Technology Development Needs," *Proceedings of the Second International Conference on Green Propellants for Space Propulsion*, Paper ESA-SP-557, ESA Publications Division, ESTEC, Noordwijk, The Netherlands, June 2004, p. 4.1.
- [2] Bombelli, V., "Economic Benefits for the Use of Non-Toxic Monopropellants for Spacecraft Applications," AIAA Paper 2003-4783, July 2003.
- [3] Anon., "Hazard Analysis of Commercial Space Transportation; Vol. 1: Operations, Vol. 2: Hazards, Vol. 3: Risk Analysis," U.S. Dept. of Transportation PB93-199040, Accession No. 00620693, 1988.
- [4] Anon., "Highly Controllable Solid Propellant and Rocket Motor Propulsion Technology," Missile Defense Agency, Small Business Innovative Research MDA05-069 (MDA), data available online at http://www.dodsbir.net/sitis/archives_display_topic.asp?Bookmark=28363[retrieved 21 Feb. 2012].
- [5] Betts, E. M., and Frederick, R., "Historical Systems Study of Liquid Rocket Engine Throttling Capabilities," AIAA Paper 2010-0863, July 2010.
- [6] Bradley, M., "Space Shuttle Main Engine Off-Nominal Low Power Level Operation," AIAA Paper 1997-2685, July 1997.
- [7] Dressler, G. A., and Bauer, J. M., "TRW Pintle Engine Heritage and Performance Characteristics," AIAA Paper 2000-3871, July 2000.
- [8] Miller, J. A., Hoffman, A., Rockow, R., Elverum, G., and Staudhammer, P., "Descent Engine for the Lunar Module," AIAA Paper 1967-521, July 1967.
- [9] Anon., "JCM Rocket Motor Achieves 20:1 Thrust Turndown," *Jane's Missiles and Rockets*, Vol. 8, No. 4, April 2004, pp. 1–2.
- [10] Giuliano, V. J., Leonard, T. G., and Lyda, R. T., "CECE: Expanding the Envelope of Deep Throttling Technology in Liquid Oxygen/Liquid Hydrogen Rocket Engines for NASA Exploration Missions," *46th AIAA/SME/SAE/ASEE Joint Propulsion Conference*, AIAA Paper 2010-6724, Nashville, TN, July 2010.
- [11] Waidmann, W., "Thrust Modulation in Hybrid Rocket Engines," *Journal of Propulsion and Power*, Vol. 4, No. 5, 1988, pp. 421–427. doi:10.2514/3.23083
- [12] Blomshield, F. S., "Lessons Learned in Solid Rocket Combustion Instability," AIAA Paper 2007-5803, July 2007.
- [13] Sutton, G. P., and Biblarz, O., *Rocket Propulsion Elements*, 7th ed., Wiley, New York, 2001, pp. 579–606.
- [14] Marxman, G., and Gilbert, M., "Turbulent Boundary Layer Combustion in the Hybrid Rocket," *Ninth Symposium on Combustion*, Academic Press, New York, 1963, pp. 371–383.
- [15] Marxman, G. A., Wooldridge, C. E., and Muzzy, R. J., "Fundamentals of Hybrid Boundary Layer Combustion," *Heterogeneous Combustion*, edited by Wolfard, H. G., Glassman, I., and Green, L. Jr., Vol. 15, Progress in Astronautics and Aeronautics, Academic Press, New York, 1964, pp. 485–522.
- [16] Strand, L. D., Ray, R. L., and Cohen, N. S., "Hybrid Rocket Combustion Study," AIAA Paper 93-2412, June 1993.
- [17] Chiaverini, M. J., Kuo, K. K., Peretz, A., and Harting, G., "Regression-Rate and Heat-Transfer Correlations for Hybrid Rocket Combustion," *Journal of Propulsion and Power*, Vol. 17, No. 1, 2001, pp. 99–110. doi:10.2514/2.5714
- [18] Eilers, S. D., and Whitmore, S. A., "Correlation of Hybrid Rocket Propellant Regression Measurements with Enthalpy-Balance Model Predictions," *Journal of Spacecraft and Rockets*, Vol. 45, No. 4, 2008, pp. 1010–1020. doi:10.2514/1.33804
- [19] Peterson, Z. W., Eilers, S. A., and Whitmore, S. A., "Analytical and Experimental Comparisons of HTPB and ABS as Hybrid Rocket Fuels," AIAA Paper 2011-5909, 2011.
- [20] Bath, A., "Performance Characterization of Complex Fuel Port Geometries for Hybrid Rocket Fuel Grains," M.S. Thesis, Dept. of Mechanical and Aerospace Engineering, Utah State Univ., Logan, UT, Dec. 2012.
- [21] Peterson, Z. W., Eilers, S. D., and Whitmore, S. A., "Closed-Loop Pressure Throttling of a Nitrous-Oxide HTPB Hybrid Rocket Motor," AIAA Paper 2012-4200, 2012.
- [22] Kuo, K. K., and Chiaverini, M. J., *Fundamentals of Hybrid Rocket Combustion and Propulsion*, Progress in Astronautics and Aeronautics, AIAA, Reston, VA, 2007, pp. 351–366.
- [23] Hunt, C. R., Phillips, O. M., and Williams, D. (eds.), "Turbulence and Stochastic Processes: Kolmogorov's Ideas 50 Years On," *Proceedings of the Royal Society of London*, Vol. 434, No. 1, 1991, pp. 1–240.
- [24] Span, R., and Wagner, W., "Equations of State for Technical Applications. I. Simultaneously Optimized Functional Forms for Nonpolar and Polar Fluids," *International Journal of Thermophysics*, Vol. 24, No. 1, 2003, pp. 1–39.
- [25] Span, R., and Wagner, W., "Equations of State for Technical Applications. III. Results for Polar Fluids," *International Journal of Thermophysics*, Vol. 24, No. 1, 2003, pp. 111–162.
- [26] Whitmore, S. A., and Chandler, S., "Engineering Model for Saturated N₂O Propellant Feed Systems," *Journal of Propulsion and Power*, Vol. 26, No. 4, 2010, pp. 706–714. doi:10.2514/1.47131
- [27] Gordon, S., and McBride, B. J., "Computer Program for Calculation of Complex Chemical Equilibrium Compositions and Applications," NASA RP-1311, 1994.
- [28] Anderson, J. D. Jr., *Modern Compressible Flow with Historical Perspective*, 3rd. ed., McGraw-Hill, New York, 2003, pp. 65–78.
- [29] Dyer, J., Doran, E., Dunn, Z., and Lohner, K., "Modeling Feed System Flow Physics for Self-Pressuring Propellants," AIAA Paper 2007-5702, July 2007.
- [30] Peterson, Z. W., Eilers, S. D., and Whitmore, S. A., "Closed-Loop Pressure Throttling of a Nitrous-Oxide HTPB Hybrid Rocket Motor," AIAA Paper 2012-4200, 2012.

E. Kim
Associate Editor